

ACCEPTED MANUSCRIPT

## Intrinsic characteristics of Si solar cells coated with thick luminescence down-shifting sol-gel glass films

To cite this article before publication: Yuki Idutsu *et al* 2023 *Jpn. J. Appl. Phys.* in press <https://doi.org/10.35848/1347-4065/acc03e>

### Manuscript version: Accepted Manuscript

Accepted Manuscript is “the version of the article accepted for publication including all changes made as a result of the peer review process, and which may also include the addition to the article by IOP Publishing of a header, an article ID, a cover sheet and/or an ‘Accepted Manuscript’ watermark, but excluding any other editing, typesetting or other changes made by IOP Publishing and/or its licensors”

This Accepted Manuscript is © 2023 The Japan Society of Applied Physics.

During the embargo period (the 12 month period from the publication of the Version of Record of this article), the Accepted Manuscript is fully protected by copyright and cannot be reused or reposted elsewhere.

As the Version of Record of this article is going to be / has been published on a subscription basis, this Accepted Manuscript is available for reuse under a CC BY-NC-ND 3.0 licence after the 12 month embargo period.

After the embargo period, everyone is permitted to use copy and redistribute this article for non-commercial purposes only, provided that they adhere to all the terms of the licence <https://creativecommons.org/licenses/by-nc-nd/3.0>

Although reasonable endeavours have been taken to obtain all necessary permissions from third parties to include their copyrighted content within this article, their full citation and copyright line may not be present in this Accepted Manuscript version. Before using any content from this article, please refer to the Version of Record on IOPscience once published for full citation and copyright details, as permissions will likely be required. All third party content is fully copyright protected, unless specifically stated otherwise in the figure caption in the Version of Record.

View the [article online](#) for updates and enhancements.

# Intrinsic characteristics of Si solar cells coated with thick luminescence down-shifting sol-gel glass films

Yuki Idutsu<sup>1</sup>, Keigo Awai<sup>2</sup>, Jianbo Liang<sup>1</sup>, Hisaaki Nishimura<sup>1</sup>, DaeGwi Kim<sup>1</sup>, Yong-Gu Shim<sup>3</sup> and Naoteru Shigekawa<sup>1\*</sup>

<sup>1</sup>Graduate School of Engineering, Osaka Metropolitan University, Osaka 558-8585, Japan

<sup>2</sup>Graduate School of Engineering, Osaka City University, Osaka 558-8585, Japan

<sup>3</sup>Graduate School of Engineering, Osaka Metropolitan University, Osaka 599-8531, Japan

We investigate effects of several-hundred-micron thick luminescence down-shifting (LDS) films composed of sol-gel glass with Zn-based nanoparticles (NPs) dispersed on characteristics of Si solar cells. Their internal quantum efficiencies (IQEs) are successfully measured by separating contributions of downshifted photons in measuring reflectance for 300-400 nm, wavelengths of incident photons absorbed by the NPs. We find that IQEs for this wavelength range are more enhanced by employing thicker LDS films, i.e., LDS films with higher optical densities. We also discuss relationship among the number density of NPs in LDS films, their optical properties, and IQEs of cells. We observe a discrepancy between measured and calculated IQEs and indicate escape of downshifted photons across sides of LDS films as its possible origin.

## 1. Introduction

Given that photovoltaics (PVs) are promising as renewable energy source, reduction of the loss in conversion from solar energy to electricity is strongly requested. Luminescence down-shifting (LDS)<sup>1-9)</sup> or luminescence down-conversion (LDC)<sup>10-12)</sup> are assumed to improve the spectral response (SR) of cells in ultraviolet (UV) region and reduce the loss in the UV wavelength range since the incident UV photons are absorbed, and the emitted visible photons can penetrate more deeply into the cells.<sup>13)</sup> UV-induced degradation in perovskite-based PVs and ethylene vinyl acetate (EVA) films in PV modules can be suppressed by applying LDS or LDC effects.<sup>14)</sup>

Several types of LDS materials were applied for Si,<sup>1-3)</sup> III-V,<sup>4,5)</sup> and perovskite<sup>6-8)</sup> single and multi-junction<sup>9)</sup> solar cells. Substances with a large Stokes shift, a high quantum efficiency, an excellent photostability, and manipulable absorption and emission wavelengths are preferable as LDS materials. Organic dyes<sup>3,15)</sup> and rare-earth-doped complexes<sup>1,2,16-19)</sup> are

\*Email: shigekawa@omu.ac.jp

promising for LDS materials applied for solar cells. Semiconductor nanoparticles (NPs) are also widely applied as LDS materials since their optical absorption and emission spectra can be tuned by varying their size and changing doped species. Cd and Zn-related,<sup>20–22)</sup> carbon-related<sup>23)</sup> and perovskite<sup>24,25)</sup> NPs were utilized for improving the quantum efficiency of Si cells. These semiconductor NPs were mainly synthesized by hot injection method.<sup>26)</sup> The prepared NPs were hydrophobic, and were dispersed in organic solvents when they were used as LDS materials.<sup>27)</sup>

Thicker LDS films, i.e., LDS films with higher optical densities are preferable for more markedly improving solar cell characteristics. Several-hundred-micron thick LDS films are fabricated by dispersing LDS materials in films made of EVA<sup>3,17,19,24)</sup>, polymethyl methacrylate (PMMA)<sup>16,22)</sup> or silica glass.<sup>18)</sup> Organic solvents such as toluene were used in forming EVA and PMMA films. Effects of such LDS films on solar cells were argued based on their external quantum efficiencies (EQEs) in the most of the forementioned works. This means that the two types of contribution of LDS films—reduction in reflectance at the surface of fabricated LDS films and the intrinsic LDS effects—were simultaneously investigated. We previously deposited Zn-based core/shell NPs on Si cells using the layer-by-layer (LBL) method.<sup>28)</sup> The thickness of deposited films was  $\sim 100$  nm. By examining the internal quantum efficiency (IQE) of cells, we directly observed the enhancement of their SR in the UV wavelength region due to the LDS of NPs. An analytical model for the relationship between IQEs of cells and optical densities (ODs) of LBL-based LDS films was proposed, and the results of calculations were compared with measurements.

In this work, we investigated the intrinsic effects of thick ( $> 500$   $\mu\text{m}$ ) LDS films on SR of Si cells in the UV wavelength region as the first step for precisely grasping roles of LDS films and enabling to design them. The LDS films were prepared by applying sol-gel process of water soluble silica-based matrices and dispersing hydrophilic ZnSe/ZnS:Mn/ZnS shell-doped NPs<sup>29)</sup> that were synthesized using the hydrothermal method,<sup>30–33)</sup> i.e., without using organic solvents. It is also notable that elements composing the NPs, Zn, Se, S, and Mn, are abundant in the crust,<sup>34)</sup> and impacts on environment due to NPs are small. The wavelength of downshifted photons emitted from the NPs was  $\approx 600$  nm.<sup>29,32,33)</sup> Their photo-luminescence quantum yield (PLQY) was as high as 84%.<sup>29)</sup> The ODs of fabricated LDS films exceeded 1 in the UV wavelength region thank to thicknesses of films. This means that downshifted photons unignorablely contribute to the measured reflectance of cells in the UV wavelength region, which must be precisely determined for extracting IQE from EQE. We explored a method for removing the contribution of downshifted photons, and discussed the relationship

among intrinsic characteristics of cells and optical properties of deposited LDS films. The measured results were compared with calculation using a model that we reported.<sup>28)</sup> We also estimated the number density of NPs in the LDS films and discussed relationships among the number density of NPs, optical properties of LDS films, and solar cell characteristics.

## 2. Experiments

We synthesized ZnSe/ZnS:Mn/ZnS shell-doped NPs with a diameter of  $\sim 5$  nm.<sup>29)</sup> We prepared two aqueous solutions with different NP concentrations. ODs at the absorption peak wavelength were measured using a cell with an optical path length of 10 mm. The ODs of the two solutions were found to be 5 and 12, respectively. The density of NPs of each solution should be proportional to the measured OD.

We deposited a sol-gel glass film with NPs dispersed on the surface of a glass plate by using a reported process.<sup>29,35)</sup> For forming sol-gel glass, we prepared 6 ml sol-mixture composed of DI water, NP solution, and 3-aminopropyltrimethoxysilane (APTMS). The volume ratio was DI water:NP solution:APTMS = 4:1:2. The sol was deposited on a glass plate, and was dried under atmospheric condition to form gel. Sol-gel glass films made in combination with sparse/dense NP solutions were referred to as S2 and S3, respectively. Note that S2 and S3 should work as LDS films. We also deposited sol-gel glass without NPs on a glass plate, S1, in which LDS should not occur.

We fabricated n-on-p Si cells by implantations of B and P ions to high-resistive p-Si substrates and subsequent annealing.<sup>28)</sup> The area of emitters was 10 mm by 12 mm. Using the same conditions for preparing S1-S3, we formed a sol-gel glass film without NPs, S1', and two types of NP-dispersed sol-gel glass films, S2' and S3', on Si cells. The number density of NPs and optical properties of sol-gel glass films on Si cells were assumed to be the same as those of films on glass plates. Thicknesses of sol-gel glass films  $d$  in S1-S3 and S1'-S3' were found to be 500-800  $\mu\text{m}$  using a micrometer, as is summarized in Table I. Using Rutherford backscattering spectrometry (RBS), the concentration of Se atoms was estimated to be  $1.50 \times 10^{19} \text{ cm}^{-3}$  for S3', the sol-gel glass film with a higher NP density. No significant result for the concentration of Se was obtained for S2'.

We investigated optical characteristics such as transmittance ( $T$ ), photoluminescence (PL) spectra, the absolute PLQY and refractive index of sol-gel glass films. The  $T$  spectra were obtained using a JASCO V-650 UV-Vis spectrophotometer with a spectral resolution of 0.5 nm. The PL spectra were measured with a JASCO FP-8300 spectrofluorometer with spectral resolution of 0.5 nm. A monochromatic output of Xe lamp ( $\lambda = 325$  nm) was used for PL

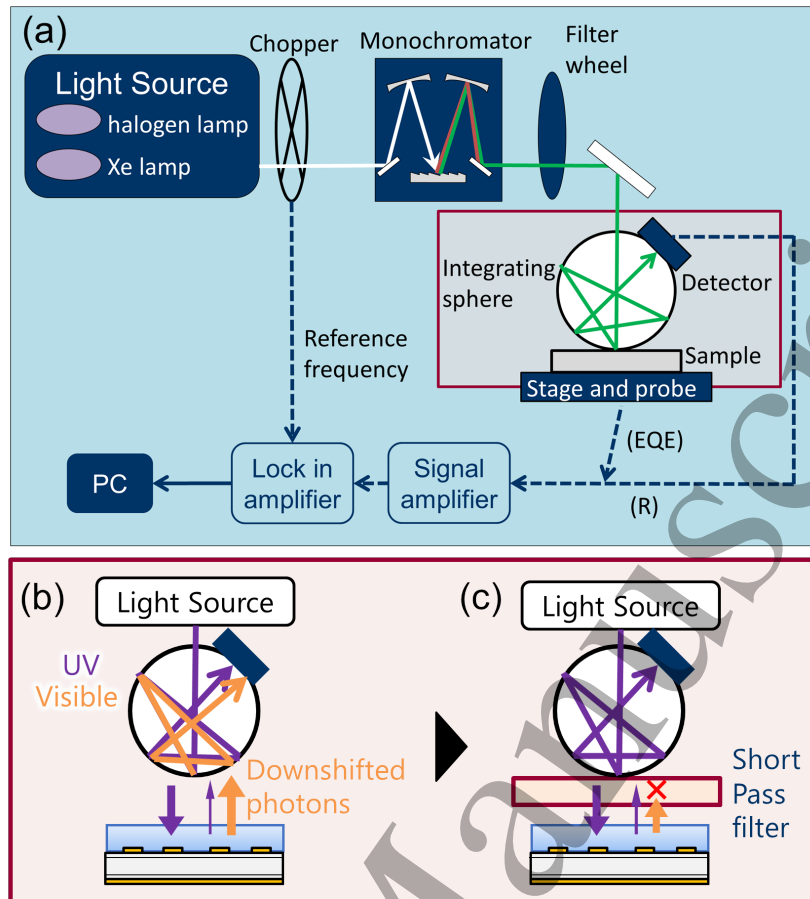


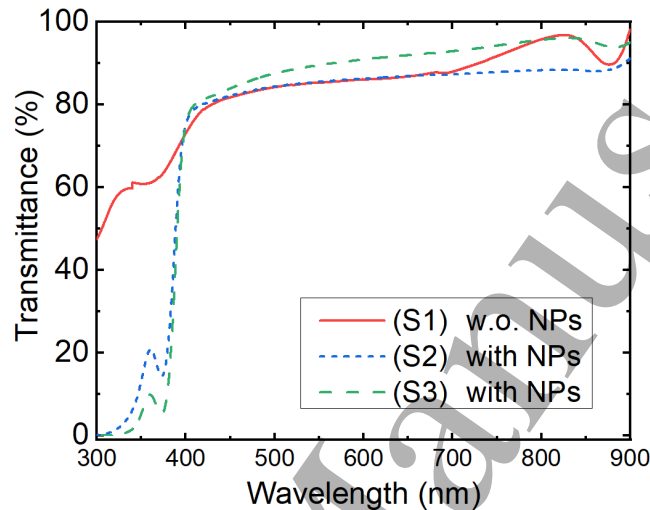
**Fig. 1.** (a) Measurement diagram of EQE and reflectance. Optical path for reflectance measurement (b) without or (c) with short pass filter.

1 measurement. The absolute PLQY, or the ratio of integrated PL intensity to absorption of  
 2 incident light, was measured for the incident light with  $\lambda$  between 300 and 400 nm. A JASCO  
 3 ILF-835 100 mm integrating sphere system coupled with the spectrofluorometer was used in  
 4 PLQY measurement. The refractive index was evaluated by ellipsometric measurements.

5 We measured current-voltage ( $I - V$ ) characteristics of S1'-S3' under the solar irradiance  
 6 of AM1.5G/one sun using an in-house solar simulator as well as their reflectance ( $R$ ) and EQE  
 7 characteristics at room temperature. Si cells without sol-gel glass films were also charac-  
 8 terized as reference. In our facility for reflectance and EQE measurements, the reflected light  
 9 from cell surfaces was guided to the detector, as is shown in Fig. 1(a). We placed a short pass  
 10 filter with 50% transmittance at  $\approx 385$  nm (Sigmakoki UTVAF-50S-33U) on the top of cells  
 11 in measuring their reflectance for separating the contribution of downshifted visible photons  
 12 from the reflectance in a UV wavelength region. The diagrams for reflectance measurement  
 13 without and with the short pass filter are shown in Figs. 1(b) and 1(c), respectively.

**Table I.** Nominal thicknesses of sol-gel glass films with or without NPs measured by micrometer.

Sample	$d$ ( $\mu\text{m}$ )	Sample	$d$ ( $\mu\text{m}$ )
S1	$550\pm 50$	S1'	$520\pm 50$
S2	$684\pm 50$	S2'	$803\pm 50$
S3	$655\pm 50$	S3'	$510\pm 50$

**Fig. 2.**  $T$  spectra of sol-gel glass films formed on glass plates, S1-S3.

### 3. Results

The  $T$  spectra of S1-S3 are shown in Fig. 2.  $T$  of the three samples was commonly  $> 80\%$  for visible photons with  $\lambda > 400$  nm. Their  $T$  was lower in the UV wavelength region. For  $\lambda < 400$  nm,  $T$  of S1 was  $\sim 60\%$ , and S2 and S3 revealed a smaller transmittance in comparison with S1.  $T$  of S3 at 350 nm was 5.2%. PL spectra of these sol-gel glass films are shown in Fig. 3. We observed peaks at 600 nm in the PL spectra of S2 and S3. PL signal of S3 was approximately twice as large as that of S2. PLQY spectra of S2 and S3 are shown in Fig. 4. The PLQY of S2, 51.8% for 350 nm, was slightly lower than that of S3, 61.5% for the same  $\lambda$ . The refractive indices of S1-S3 are shown in Fig. 5(a). They are compared with those of ZnS<sup>36)</sup> and ZnSe<sup>37)</sup> in Fig. 5(b). The refractive indices of S1-S3 were close to one another, and they were much smaller than those of ZnSe and ZnS.

Results of the transmittance measurements implied that the absorption of S1, sol-gel glass film without NPs, was apparent for  $\lambda < 400$  nm. This means that both of the sol-gel glass and NPs contributed to  $T$  of S2 and S3. The smaller  $T$  for  $\lambda < 400$  nm and stronger PL signal of

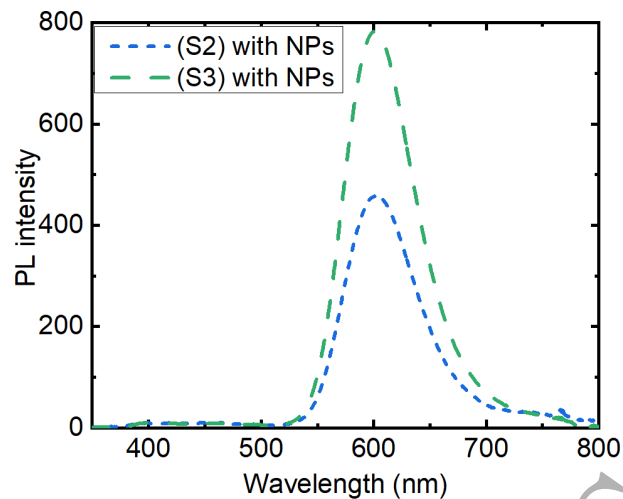


Fig. 3. PL spectra of sol-gel glass films with NPs dispersed, S2 and S3.

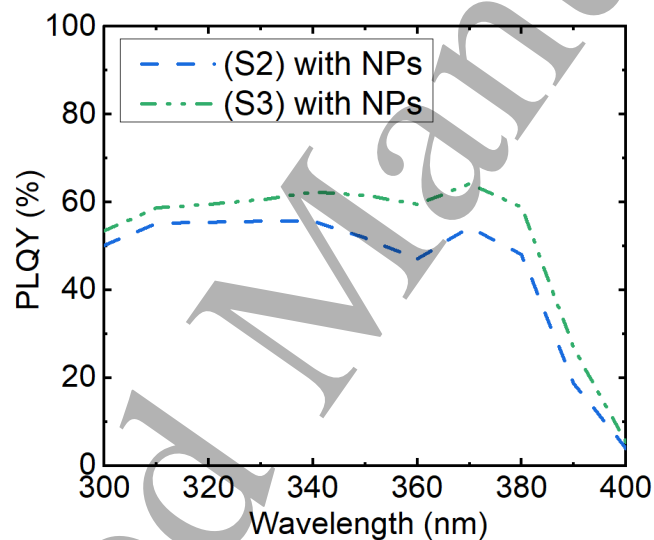
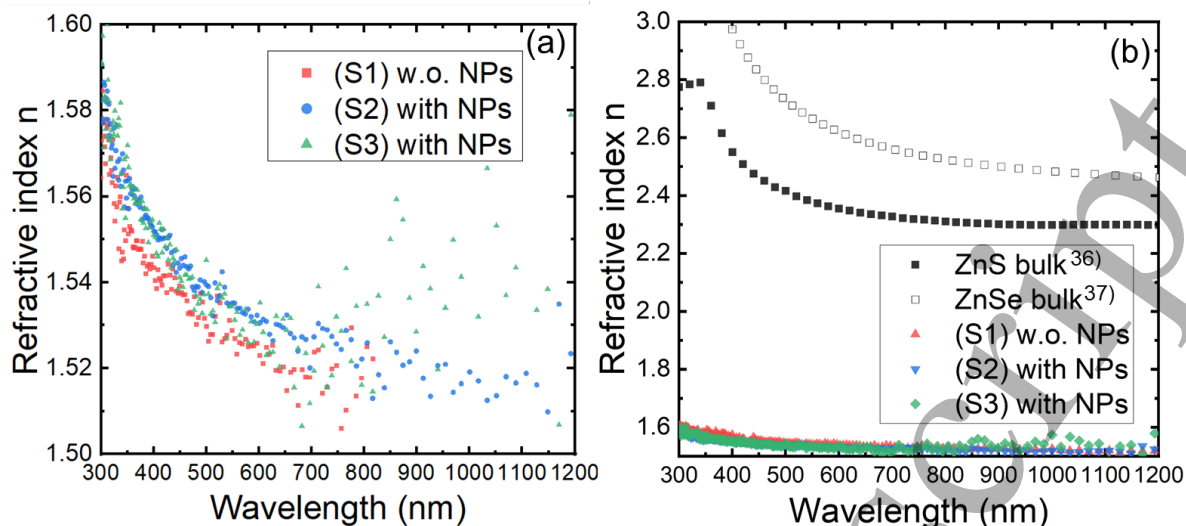


Fig. 4. PLQY spectra of S2 and S3.

1 S3 in comparison with those of S2 were attributed to the higher number density of NPs in S3.  
 2 Given that the optical properties of a single NP in S2 and S3 were assumed to be the same,  
 3 the observed lower PLQY of S2 was likely to be attributable to the absorption of sol-gel glass,  
 4 which did not bring about LDS.

5 The  $I-V$  characteristics of S1'-S3' are shown in Fig. 6. Characteristics of reference cell are  
 6 also shown for comparison. Parameters extracted from the respective curves—short-circuit  
 7 current ( $J_{sc}$ ), open-circuit voltage ( $V_{oc}$ ), fill factor, series and shunt resistances ( $R_s$  and  $R_{sh}$ ),  
 8 and conversion efficiency ( $\eta$ )—are summarized in Table II. We obtained a larger  $J_{sc}$  and a



**Fig. 5.** (a) Refractive indices of S1-S3. (b) Comparison of refractive indices of S1-S3 with those of bulk ZnS<sup>36)</sup> bulk and ZnSe bulk.<sup>37)</sup>

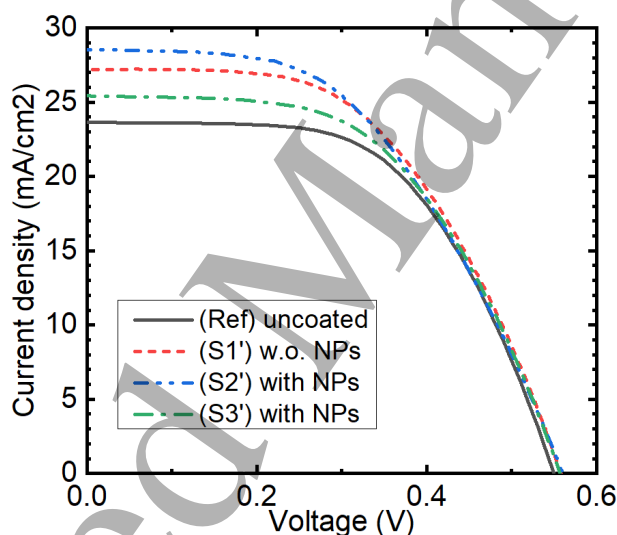


**Fig. 6.**  $I - V$  characteristic of S1'-S3' under the AM 1.5G/one sun solar irradiance.  $I - V$  characteristics of an uncoated cell (reference) are also shown for comparison.

1 higher  $\eta$  in S1'-S3' in comparison with reference cell. The surface of S3' was not entirely  
 2 covered by the sol-gel glass film, which might be the origin of its lower  $J_{sc}$  in comparison with  
 3 those of S1' and S2'.  $V_{oc}$  and  $R_s$  in S1'-S3' ( 0.55-0.56 V and 2.84-3.55  $\Omega \cdot \text{cm}^2$ ) was close to  
 4 that of reference cell (0.55 V and 2.66  $\Omega \cdot \text{cm}^2$ ). The degradation in  $R_{sh}$  in S1'-S3' might be  
 5 related to possible damage on the sides of the cell introduced during depositing sol-gel glass  
 6 films. However, the reduced  $R_{sh}$  was still high enough and its impacts on cell characteristics  
 7 were negligibly small.

**Table II.** Parameters of Si cell characteristics.

	Reference	S1'	S2'	S3'
$J_{sc}$ (mA/cm <sup>2</sup> )	23.6	28.1	28.5	25.4
$V_{oc}$ (V)	0.55	0.56	0.56	0.55
Fill Factor	0.57	0.51	0.49	0.54
$R_s$ ( $\Omega \cdot \text{cm}^2$ )	2.66	3.13	3.55	2.84
$R_{sh}$ ( $10^3 \Omega \cdot \text{cm}^2$ )	22.0	1.01	0.65	0.85
$\eta$ (%)	7.41	8.00	7.80	7.64

$R$  spectra of S1'-S3' measured without and with short pass filter are shown in Figs. 7(a) and 7(b), respectively. Based on the assumption that optical properties of sol-gel glass films on Si cells were same as those of films on glass plates, we calculated the reflectance of S1'-S3' using the refractive indices and extinction coefficients of S1-S3 and Si.<sup>38)</sup> The extinction coefficients of S1-S3 were estimated using the step described in the next section. To consider effects of the spatial fluctuation of thickness of sol-gel glass films, we varied  $d$  in the range of  $\pm 50 \mu\text{m}$ , and averaged the calculation results over  $d$ .

The calculated  $R$  is also shown in these figures for comparison.  $R$  of S2' and S3' measured without using the short pass filter diverged for  $\lambda < 350 \text{ nm}$  because of the contribution of downshifted photons. The measured  $R$  using the short pass filter, in contrast, is stable and close to the calculation, which suggests the validity of the approach employed in measuring reflectance in the UV wavelength region. We also found that  $R$  of S1'-S3' was lower than that of the reference cell in the entire wavelength region (not shown).

Figures 8 shows the EQE spectra of S1'-S3' and a reference cell for  $\lambda$  between 300 and 1200 nm. The enhanced EQE of S1'-S3' for  $\lambda > 400 \text{ nm}$ , which is the origin of increase in  $J_{sc}$  (Table II), is explained using a scheme that the sol-gel glass films worked as anti-reflection layers since sol-gel glass films with and without NPs brought about similar EQEs for  $\lambda > 400 \text{ nm}$ .

Using the EQE and reflectance spectra (Fig. 7(a)), we extracted IQEs of S1'-S3' and the reference cell, which are shown in Fig. 9. We observed IQE enhancement for 300-400 nm in S2' and S3' in comparison with IQE of S1'. The IQE of S3' was approximately 16% higher than that of reference cell at around 350 nm. The difference in the IQE spectra for  $\lambda > 400 \text{ nm}$  among cells was not apparent, in contrast to the difference observed in the EQE spectra.

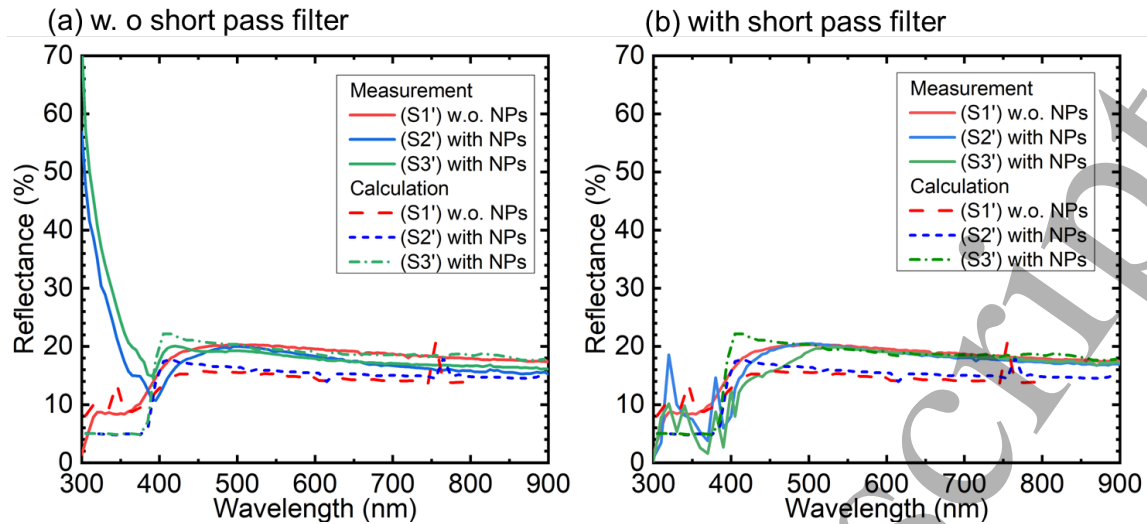


**Fig. 7.**  $R$  spectra of  $S1'$ - $S3'$  measured (a) without and (b) with the short pass filter. Calculated results are also shown.

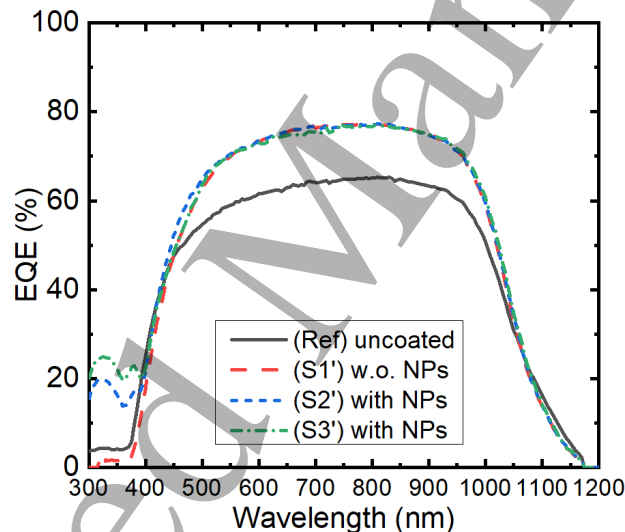


**Fig. 8.** EQE spectra of  $S1'$ - $S3'$ . The spectrum for an uncoated cell (reference) is also shown for comparison.

#### 4. Discussion

We discuss relationships among the number density of NPs in LDS films, their optical properties, extinction coefficient and OD, and IQE of cells in the UV wavelength region. We start with calculation of the number density of NPs by using the following assumptions.

- (1) All of Se atoms in sol-gel glass films are distributed in cores of NPs.
- (2) The diameter of ZnSe cores is 5 nm.
- (3) ZnSe in the cores reveals the zincblende structure with the same lattice constant as that

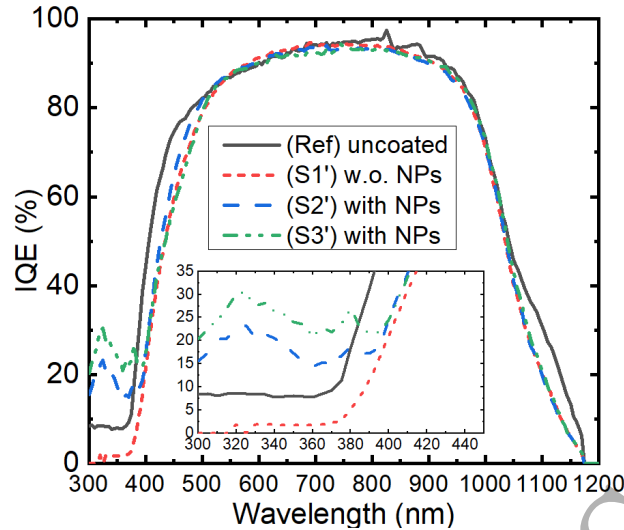


**Fig. 9.** IQE spectra of S1'-S3'. The spectrum for an uncoated cell (reference) is also shown for comparison. In the inset is shown the spectra for the UV wavelength region.

of bulk ZnSe crystals in literature (5.6687 Å).

(4) The densities of NPs in LDS films on glass plates are the same as those in films on cells as aforementioned.

Based on the above assumptions, we obtained the number density of NPs in S3 as  $1.1 \times 10^{16} \text{ cm}^{-3}$ . The number density of NPs of S2 was estimated to be  $4.4 \times 10^{15} \text{ cm}^{-3}$  based on the OD of NP solutions and the mixing ratio of materials in gel process.

The extinction coefficient of S1-S3,  $k_i$  for Si ( $i = 1 - 3$ ), is given by

$$k_i = \frac{\lambda \text{IOD}}{4\pi d} \ln(10), \quad (1)$$

using the IOD (intrinsic OD) of each sol-gel glass film, which is defined as  $\text{IOD} = -\log_{10}(T/(1-R))$ . Noting that S1, a sol-gel glass film without NPs, also revealed optical absorption in the UV region,  $k$  due to NPs in S2 and S3,  $k_{\text{NP},2}$  and  $k_{\text{NP},3}$ , is given by

$$k_{\text{NP},i} = k_i - k_1 \text{ for } i = 2 \text{ and } 3. \quad (2)$$

It was reported that NPs were periodically aligned in LBL-based LDS films.<sup>39)</sup> The in-plane and out-of-plane separations between centers of 5-nm NPs are estimated to be 5 nm and 5.5 nm, respectively, which means that the number density of NPs in a 140-nm thick LBL-based LDS film, which we previously reported,<sup>28)</sup> is  $6.0 \times 10^{18} \text{ cm}^{-3}$ . Given that the IOD of this LDS film was 0.07 at 350 nm, the extinction coefficient at 350 nm was  $3.30 \times 10^{-2}$ . The thickness, IOD, extinction coefficient, and number density of NPs for each LDS film are summarized in Table III. Relationship among these parameters are useful in designing LDS

**Table III.** Optical properties at 350 nm of LDS films. The number density of NPs estimated for the respective films are also shown. Number densities of S2 and S3 are based on RBS measurement of S3'. That for LBL-based LDS film is based on the nominal separation between centers of NPs in the film.

LDS film	$d$	IOD at 350 nm	$k_{\text{NP}}$ at 350 nm	Number density of NPs
S2	684 $\mu\text{m}$	0.88	$5.76 \times 10^{-5}$	$4.4 \times 10^{15} \text{ cm}^{-3}$
S3	655 $\mu\text{m}$	1.28	$1.00 \times 10^{-4}$	$1.1 \times 10^{16} \text{ cm}^{-3}$
LBL-based <sup>28)</sup>	140 nm	0.07	$3.30 \times 10^{-2}$	$6.0 \times 10^{18} \text{ cm}^{-3}$

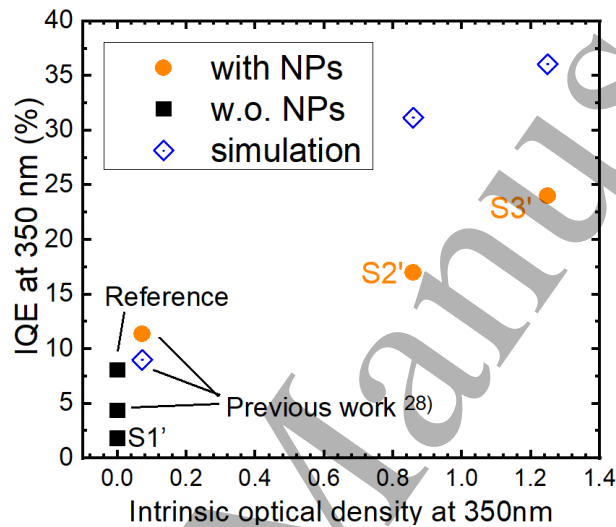


**Fig. 10.** IOD-IQE relationships of Si cells coated with sol-gel glass LDS films, S1'-S3', a cell coated with a 140-nm-thick LBL-based LDS film,<sup>28)</sup> and an uncoated cell (as reference). Calculated IQEs for coated cells are also shown.

1 films. Although the number density of NPs hence the extinction coefficient of sol-gel glass  
 2 based LDS films, S2 and S3, are  $\approx 1/100 - 1/1000$  of those of the LBL-based LDS film,  
 3 the sol-gel glass based films outperform the LBL-based film because of a large ( $> 1000$ )  
 4 difference in thicknesses.

5 The absorption cross section for  $\lambda$  of 350 nm was estimated to be 0.47, 0.33, and 0.20  $\text{nm}^2$   
 6 for S2, S3, and the LBL-based LDS film, respectively, by combining the number density of  
 7 NPs and  $k_{\text{NP}}$  at this wavelength. The difference in absorption cross sections among LDS films  
 8 might be due to more marked shadow effects of overlapping NPs in LDS films with higher  
 9 NP densities. It is also notable that the estimated cross section was  $\sim 1/100-1/40$  of 19.6  $\text{nm}^2$ ,  
 10 the cross section of NPs with a diameter of 5 nm.<sup>29)</sup>

11 Figure 10 shows the relationship between IQE at 350 nm of S1'-S3' and IOD of S1-S3

**Table IV.** Calculation of fraction of downshifted photons that reach to Si substrate for S2' and S3'.

Cell type	$d$	$N_1$	$\eta_c$
S2'	803 $\mu\text{m}$	$1.53 - 0.000014j$	0.62
S3'	510 $\mu\text{m}$	$1.54 - 0.000009j$	0.62

at 350 nm. Results for Si cells coated with a 140-nm-thick LBL-based LDS film are also shown. Larger IQEs at 350 nm were observed for Si cells coated with LDS films with higher ODs at this wavelength, i.e., LDS effects on solar cell characteristics were more enhanced by increasing amount of NPs in LDS films. Reflections due to UV photon at wavelengths of 300-350 nm were cut off by the filter, so the IQE enhancement derived from the emission of the NPs was surely observed, i.e., the method for experimentally investigating intrinsic effects of high-OD LDS films on solar cells was established.

IQE of cells coated with LDS films in the UV wavelength region should given by the sum of contributions of incident UV photons and downshifted photons emitted from NPs, i.e., IQE of cells coated with LDS films at 350 nm,  $\text{IQE}_{350,\text{NP}}$ , is expressed as<sup>28)</sup>

$$\text{IQE}_{350,\text{NP}} = \frac{T_{350}}{1 - R_{350}} \times \text{IQE}_{350,\text{ref}} + \left(1 - \frac{T_{350}}{1 - R_{350}}\right) \times \text{PLQY} \times \eta_c \times \text{IQE}_{\lambda_{\text{LDS}},\text{ref}}, \quad (3)$$

using the transmittance of incident 350 nm photons across the LDS layer on Si,  $T_{350}$ , their reflectance,  $R_{350}$ , IQEs of uncoated cells at 350 nm and at  $\lambda$  of downshifted photons,  $\text{IQE}_{350,\text{ref}}$  and  $\text{IQE}_{\lambda_{\text{LDS}},\text{ref}}$ . As we previously reported,<sup>28)</sup>  $T_{350}/(1 - R_{350})$  and  $(1 - T_{350}/(1 - R_{350})) \times \text{PLQY}$  provide the ratio of the flux of 350-nm photons arriving at Si to the flux of 350-nm incident photons penetrating into the LDS film, and the ratio of the flux of downshifted photons emitted from NPs to the the flux of 350-nm incident photons penetrating into the LDS film, respectively. The coefficient  $\eta_c$  ( $0 < \eta_c < 1$ ) represents the fraction of downshifted photons that reach to the Si cell underneath. We set  $\lambda$  of downshifted photons to 600 nm, or the peak wavelength of PL spectra of sol-gel glass films.  $\eta_c$  was calculated using the complex refractive index of air ( $N_0 = 1 + 0j$ ), sol-gel glass films ( $N_1$ ), and Si ( $N_2 = 3.93 - 0.0185j$ <sup>38)</sup>) at 600 nm.  $N_1$  at 600 nm and the obtained  $\eta_c$  for S2' and S3' are shown in Table IV.

The obtained values are compared with the measured IQEs at 350 nm in Fig. 10. The calculated IQE increased as the OD of LDS film increased in accordance with the results of measurements. The calculated IQEs were, however, 13% larger than experimental results for S2' and S3'. We assume that the discrepancy might be due to escape of downshifted photons across sides of LDS films (side escape loss), which was not considered in calculation, since

1  
2  
3  
4  
5  
6  
7  
8  
9  
10  
11  
12  
13  
14  
15  
16  
17  
18  
19  
20  
21  
22  
23  
24  
25  
26  
27  
28  
29  
30  
31  
32  
33  
34  
35  
36  
37  
38  
39  
40  
41  
42  
43  
44  
45  
46  
47  
48  
49  
50  
51  
52  
53  
54  
55  
56  
57  
58  
59  
60

1 their thickness was several hundred microns in S2' and S3'. Contribution of the side escape  
2 loss is assumed to be quantitatively estimated by revising the process for calculating  $\eta_c$ . The  
3 side escape loss could be reduced by forming reflectors on sides of LDS films, or employing  
4 thinner LDS films with higher densities of NPs.

## 5 **5. Conclusion**

6 We investigated intrinsic effects of high-OD LDS films on Si cells. Several-hundred-micron  
7 thick LDS films were formed on glass plates and Si cells by depositing sol-gel glass with  
8 ZnSe/ZnS:Mn/ZnS NPs dispersed. By separating contribution of downshifted photons from  
9 the reflectance in the UV wavelength region ( $\lambda < 400$  nm), IQEs of cells coated with LDS  
10 films for the UV wavelength were successfully estimated. Their IQEs were  $\approx 20\%$  for 300-  
11 400 nm by LDS effects. The obtained IQEs were larger than that for cells coated with a  
12 thin (140 nm) LBL-based LDS film because of higher ODs of sol-gel-glass based films.  
13 We discussed relationship among IQE of cells, the extinction coefficient and the density of  
14 NPs in LDS films, which are useful in designing LDS films. IQEs obtained by a numerical  
15 analysis revealed a dependence on OD of LDS films similar to that of the measured IQEs. The  
16 discrepancy between measured and calculated IQEs (13%) might be due to the side escape  
17 loss, or escape of photons across sides of the LDS films. Possible approaches for reducing the  
18 side escape loss were also shown.

## 19 **Acknowledgment**

20 This work was partly supported by JSPS KAKENHI Grant Number JP17H03538.

## References

- 1) S. Razzaq, A. Asghar, C. Lou, H. Diao, S. Huang and Y. Yin, *J. Alloys Compd.* **907**, 164512 (2022).
- 2) K. David, K. Sovann, C. So-Hye and M. Ntwaeaborwa, *Physica B Condens.*, **576**, 411711 (2020).
- 3) J. Singh, A. Kumar, A. Jaiswal, S. Suman and R. P. Jaiswal, *Sol Energy.*, **206**, 353 (2020).
- 4) Y. Ahn, J. Kim, S. Shin, S. Ganorkar, Y. Kim, Y. Kim and S. Kim, *J. Sol. Energy Eng.*, **137**, 021011 (2015).
- 5) W.-J. Ho, W.-B. Bai, J.-J. Liu and H.-P. Shiao, *Thin Solid Films*, **660**, 651 (2018)
- 6) S. A. A. Shah, M. H. Sayyad, J. Sun and Z. Guo, *J. Rare Earths.*, **40**, 1651 (2022).
- 7) R. Tao, W. Fang, F. Li, Z. Sun and L. Xu, *J. Alloys Compd.*, **823**, 153738 (2020).
- 8) C. Chen, Y. Wu, L. Liu, Y. Gao, X. Chen, W. Bi, X. Chen, D. Liu, Q. Dai and H. Song, *Adv. Sci.*, **6**, 1802046 (2019).
- 9) S. Lee, C. U. Kim, S. Bae, Y. Liu, Y. I. Noh, Z. Zhou, P. W. Leu, K. J. Choi and J.-K. Lee, *Adv. Funct. Mater.* **32**, 204328 (2022).
- 10) B. Zheng, J. Hong, L. Lin, C. Huang, H. Chen, C. Zhang, Y. Li, J. Wang and Z. Zheng, *J. Lumin.*, **241**, 118532 (2022).
- 11) G. Yang, C. Zheng, Y. Zhu, X. Li, J. Huang, X. Xu, W. Liu, S. Cui and G. Pan, *J. Alloys Compd.*, **921**, 166097 (2022).
- 12) H. Luo, S. Zhang, Z. Mu, F. Wu, Z. Nie, D. Zhu, X. Feng and Q. Zhang, *J. Alloys Compd.*, **784**, 611 (2019).
- 13) B.S. Richards, *Sol. Energy Mater Sol. Cells*, **90**, 2329 (2006).
- 14) B. González-Díaz, M. H. Saw, C. Hernández-Rodríguez, J. Sanchiz, Y. Khoo and R. Guerrero-Lemus, *J. Mater. Sci. Eng., B*, **261**, 114763 (2020).
- 15) P. Wang, X. Yan, H. Wang, C. Luo and C. Wang, *Opt. Mater.*, **132**, 112821 (2022),
- 16) Z. Zhang, J. Ju, X. Qin, H. Yan, M. Shen and C. Chen, *Mater. Chem. Phys.*, **290**, 126599 (2022).
- 17) Y. Wang, P. Gawryszewska-Wilczynsk, X. Zhang, J. Yin and Y. Wen, *Sci. China Mater.*, **63**, 544 (2020).
- 18) T. Fukuda, S. Kato, E. Kin, K. Okaniwa, H. Morikawa, Z. Honda and N. Kamata, *Opt. Mater.*, **32**, 22 (2009).
- 19) F. Meng, Z. Dehouche, T. Ireland and G. Fern, *Prog Photovolt Res Appl.*, **27**, 640

- (2019).
- 20) L. Meng, L. Shi, Y. Ge, J. Tang, Yu Chen and H. Zhong, *Sol. Energy Mater Sol. Cells*, **220**, 110856 (2021).
- 21) J. Huang, Y. Wang, G. Fei, S. Xu, B. Wang and Z. Zeng, *Colloids Surf. A Physicochem. Eng. Asp.*, **652**, 129907 (2022).
- 22) A. Flores-Pacheco, J. Raúl Montes-Bojórquez, M. Álvarez-Ramos and A. Ayón, *Micro Nano Eng.*, **15**, 100128 (2022).
- 23) T. Lv, Y. Tang, H. Fan, S. Liu, S. Zeng and W. Liu, *Sol. Energy Mater. Sol. Cells*, **235**, 111450 (2022).
- 24) P. Song, S. Hase, S. Zhao, Z. Xu, Y. Iso, and T. Isobe, *ACS Appl. Nano Mater.*, **5**, 2522 (2022).
- 25) W. Ho, G. Li, J. Liu, Z. Lin, B. You and C. Ho, *Appl. Surf. Sci.*, **436**, 927 (2018).
- 26) P. Reiss, J. Bleuse, and A. Pron, *Nano Lett.*, **2**, 781 (2002).
- 27) C. de Mello Donegá, P. Liljeroth, and D. Vanmaekelbergh, *Small*, **1**, 1152 (2005).
- 28) Y. Idutsu, K. Awai, J. Liang, H. Nishimura, D. G. Kim, Y. G. Shim, and N. Shigekawa, *Jpn. J. Appl. Phys.*, **61**, 062004 (2022).
- 29) H. Nishimura, T. Maekawa, K. Enomoto, N. Shigekawa, T. Takagi, S. Sobue, S. Kawai, and D. G. Kim, *J. Mater. Chem. C*, **9**, 693 (2021).
- 30) Y-S. Lee, H. Bu, T. Taniguchi, T. Takagi, S. Sobue, H. Yamada, T. Iwaki, and D. Kim, *Chem. Lett.*, **45**, 878 (2016).
- 31) Y-S. Lee, K. Nakano, H-B. Bu, and D. Kim, *Appl. Phys. Express*, **10**, 065001 (2017).
- 32) H. Nishimura, Y. Lin, M. Hizume, T. Taniguchi, N. Shigekawa, T. Takagi, S. Sobue, S. Kawai, E. Okuno, and D. G. Kim, *AIP Advances*, **9**, 025223 (2019).
- 33) H. Nishimura, Y. Lin, M. Hizume, T. Taniguchi, N. Shigekawa, T. Takagi, S. Sobue, S. Kawai, E. Okuno, and D. G. Kim, *Chem. Lett.*, **48**, 1081 (2019).
- 34) M. Fleischer, *J. Chem. Educ.*, **31**, 446 (1954).
- 35) H. Bu, T. Watanabe, M. Hizume, T. Takagi, S. Sobue, S. Kawai, E. Okuno and DaeGwi Kim, *Mater. Res. Express.*, **2**, 036202 (2015).
- 36) M. R. Querry, Contractor Report, CRDEC-CR-88009 (1987).
- 37) T. Amotchkina, M. Trubetskov, D. Hahner and V. Pervak, *Appl. Opt.*, **59**, A40 (2020).
- 38) C. Schinke, P. C. Peest, J. Schmidt, R. Brendel, K. Bothe, M. R. Vogt, I. Kröger, S. Winter, A. Schirmacher, S. Lim, H. T. Nguyen, and D. MacDonald, *AIP Adv.*, **5**, 067168 (2015).
- 39) T. Lee, K. Enomoto, K. Ohshiro, D. Inoue, T. Kikitsu, K. Hyeon-Deuk, Y. Pu and D.

1  
2  
3  
4  
5 1 Kim, Nat. Commun. **11**, 5471 (2020).  
6  
7  
8  
9  
10  
11  
12  
13  
14  
15  
16  
17  
18  
19  
20  
21  
22  
23  
24  
25  
26  
27  
28  
29  
30  
31  
32  
33  
34  
35  
36  
37  
38  
39  
40  
41  
42  
43  
44  
45  
46  
47  
48  
49  
50  
51  
52  
53  
54  
55  
56  
57  
58  
59  
60

Accepted Manuscript